Journal of Power Sources 218 (2012) 435–444

Contents lists available at SciVerse ScienceDirect

Journal of Power Sources

journal homepage: www.elsevier.com/locate/jpowsour

Chemical and electrochemical recycling of the nickel, cobalt, zinc and manganese from the positives electrodes of spent Ni–MH batteries from mobile phones

V.E.O. Santos, V.G. Celante, M.F.F. Lelis, M.B.J.G. Freitas*

Federal University of Espírito Santo, Chemistry Department, Laboratory of Applied Electrochemistry, Av. Fernando Ferrari, 514, Goiabeiras 29075-910, Espírito Santo, Brazil

HIGHLIGHTS

- A recycling process was developed for the positive electrodes of Ni–MH batteries.
- Chemical and electrochemical recycling methods for the Ni, Co, Zn and Mn.
- β-$Ni(OH)_2$, $Co(OH)_2$, $Zn(OH)_2$ and Mn_3O_4 were recycled by chemical precipitation.
- The electrodeposited material contains Ni, Co, CoO, $Co(OH)_2$, and Mn_3O_4.

ARTICLE INFO

Article history:
Received 24 April 2012
Received in revised form
18 June 2012
Accepted 11 July 2012
Available online 20 July 2012

Keywords:
Nickel–metal hydride
Batteries recycling
Cobalt
Nickel
Zinc
Manganese

ABSTRACT

Chemical and electrochemical recycling methods for the Ni, Co, Zn and Mn from the positives electrodes of spent Ni–MH batteries were developed. The materials recycled by chemical precipitation have the composition β-$Ni(OH)_2$, $Co(OH)_2$, $Zn(OH)_2$ and Mn_3O_4. The powder retains sulphate, nitrate and carbonate anions from the mother solution as well as adsorbed water. Studies using cyclic voltammetry show that the current density decreases for scan rates greater than 10 mV s^{-1} because of the formation of hydroxide films. The amounts of Ni^{2+}, Co^{2+}, Zn^{2+} and Mn^{2+} were obtained by analysis of the solution using the inductively coupled plasma with optical emission spectroscopy technique, which demonstrated that the electrodeposition method exhibits anomalous behaviour. The amount of deposited nickel ions is related to the composition of the sulfamate bath. The presence of manganese in the electrodeposits is due to the precipitation of $Mn(OH)_2$, and $Zn(OH)_4^{2-}$ does not undergo reduction in the investigated potential range. The electrodeposited material contains Ni, Co, CoO, $Co(OH)_2$, and Mn_3O_4. A charge efficiency of 83.7% was attained for the electrodeposits formed by the application of −1.1 V vs. Ag/AgCl at a charge density of −90 C cm^{-2}. The dissolution of the electrodeposits depends on the applied potential.

© 2012 Elsevier B.V. All rights reserved.

1. Introduction

The lead–acid, nickel–cadmium (Ni–Cd), nickel–metal hydride (Ni–MH), and Li-ion technologies are the most important battery systems. Lead–acid batteries are used when the battery weight is not significant. Nickel–cadmium batteries were invented by Edison and Junger at the beginning of the nineteenth century. The Ni–MH system was developed in 1989 for the replacement of portable Ni–Cd batteries in many applications, particularly in northern Europe, because of the toxic properties of cadmium. The newer battery technologies are based on the metals lanthanum, neodymium, nickel and cobalt, which impact the environmental to a lesser extent than cadmiun. A Ni–MH cell consists of four major components: a negative metal hydride electrode, a positive nickel electrode, a plastic separator, and an alkaline electrolyte. The active material of the negative electrode is composed of a hydrogen storage alloy that can absorb hydrogen. The alloy and a conducting agent are pasted into a nickel or nickel-plated steel substrate, which acts as a current collector and as a physical support for the active material. Two general classes of metallic alloys have been identified for battery use: mixtures of rare-earth element (REE) alloys, the so-called mischmetals, designated as AB_5 alloys, where A = La, Nd, Ce, or Pr and B = Ni, Co, Mn, or Al, and alloys that consist primarily of titanium and zirconium, designated as AB_2 alloys, where A = Ti or Zr and B = Ni, V, Cr, or Mn. The positive electrode generally consists of a porous nickel substrate that is impregnated with nickel hydroxide as the main active material. The substrate acts as a mechanical support for the active material and as a current

* Corresponding author. Tel.: +55 27 33352486; fax: +55 27 33352460.
E-mail address: marcosbj@hotmail.com (M.B.J.G. Freitas).

0378-7753/$ – see front matter © 2012 Elsevier B.V. All rights reserved.
http://dx.doi.org/10.1016/j.jpowsour.2012.07.024

collector. The addition of small amounts of cobalt, calcium, and zinc improves the capacity of the electrode. The first commercial secondary Li-ion cell was produced by Sony in 1991; since then, the use of this battery has grown rapidly because of its high energetic density. The Li-ion battery has replaced the Ni–MH battery in numerous applications, including mobile phones. Ni–MH batteries have become unsuitable for use in electronic devices and are being discarded in household wastes[1–5]. The use of recycled materials from these batteries can decrease waste contamination.

The methods of battery recycling are classified as pyrometallurgical or hydromettalurgical. Because of the large amount of metals present in Ni–MH batteries, a hydrometallurgical process is more appropriate than a pyrometallurgical process for their recycling. Hydrometallurgical recycling involves the leaching of scraps in acid or base to solubilize the metals. The metals can then be recovered either by precipitation, solvent extraction, or electrodeposition [6–15]. Alloys that contain Ni and Co produced by electrodeposition, for example, can be recycled via the electrocatalytic hydrogen evolution reaction in an alkaline medium. Because Ni–MH batteries are a recent technology, methods for their recycling are still under development. In this work, chemical and electrodeposition processes were developed for the recovery of the nickel, cobalt, zinc and manganese of spent Ni–MH batteries from mobile phones. The materials were characterized with the aid of X-ray diffraction (XRD), scanning electron microscopy (SEM), energy dispersive X-ray spectroscopy (EDS), Fourier-transform infrared spectroscopy (FT–IR), thermogravimetric analysis (TGA) and inductively coupled plasma with optical emission spectroscopy (ICP-OES).

2. Experimental

2.1. Precipitation of materials from a solution of dissolved Ni–MH batteries

In the process of chemical dissolution, 10 g of the cathode material was dissolved in 500 mL of 0.500 mol L^{-1} HNO_3 under constant agitation. After dissolution, the solutions were filtered to remove insoluble graphite and plastics. A solution of 5.0 mol L^{-1} NaOH was slowly added to the filtrate at a rate of 0.2 mL min^{-1} under constant stirring until a pH of 9.0 was achieved at a temperature of 5 °C. After being precipitated, the recovered materials were filtered, washed and stored dry.

2.2. Electrochemical recycling

2.2.1. Preparation of electroplating baths

The materials were electrodeposited from a bath prepared by dissolving 10.0 g of the positive electrode in 500 mL of 0.5 mol L^{-1} H_2SO_4. NaOH was added to the working solution until the pH was 1.5; additionally, 0.4 mol L^{-1} H_3BO_3 (as a buffering agent) and 0.3 mol L^{-1} ammonium sulfamate (as a complexing agent) were added.

2.3. Electrochemical cell

The working electrode was prepared from high-purity aluminium (Merck 99.99% w w^{-1}) with an area of 0.5 cm^2. The remainder of the electrode surface was isolated from the solution with a rapid-curing epoxy resin (Araldite) to prevent edge effects. The aluminium electrodes were polished with 400- and 600-grit abrasive papers and were subsequently washed and degreased with acetone. The polishing removes the surface layer of aluminium oxide, which is again formed spontaneously. Lastly, the electrodes were washed with distilled water and dried with hot air. A platinum electrode with a geometric area of 3.75 cm^2 was used as the counter electrode, and an Ag/AgCl electrode saturated with 3.0 mol L^{-1} KCl was used as the reference electrode. All electrochemical measurements were performed using an AUTOLAB PGSTAT 302N. The electrochemical behaviour of the metal ions in the working solution from the cathode of exhausted Ni–MH batteries was investigated using the cyclic voltammetry technique. The voltammetric studies were performed with different scanning rates of 1.0 mV s^{-1}, 5.0 mV s^{-1}, 10.0 mV s^{-1}, 20.0 mV s^{-1}, 30.0 mV s^{-1}, 40.0 mV s^{-1} and 50.0 mV s^{-1}. For all cyclic voltammetry experiments, the scans were started from an open-circuit potential of −0.73 V to a cathodic potential of −1.5 V, following an anodic region up to 1.0 V. After reaching a potential of 1.0 V, the potential scan was again returned to a potential of −0.73 V. The potentiostatic measurements of the reduction of the metal ions were performed at a constant potential of −0.9 V, −1.1 V, or −1.2 V and at a fixed charge density of 90 C cm^{-2}.

2.4. Characterization techniques

X-ray diffraction (XRD) was performed on a Shimadzu XRD-6000 model 20013 diffractometer equipped with a Cu Kα radiation source and a Ni filter, which corresponded to a wavelength of 1.540 Å. The micrographs were obtained by electron microscopy performed on a Shimadzu model SSX-50 scanning electron microscope using secondary electrons. The low-energy secondary electrons (approximately 50 eV) emerged at a depth of 100–200 Å. Thermogravimetric analysis (TGA) was performed using a TA Instruments thermobalance, model SDT Q600 V20.9, Build 20. All samples were subjected to an atmosphere of N_2 gas at a rate of 100 mL min^{-1}. The samples were scanned over the range from 25 °C to 1200 °C at a heating rate 10 °C min^{-1}. Alumina crucibles were used as sample holders during the thermal analyses. The analyses using inductively coupled plasma with optical emission spectroscopy (OES-ICP) were performed on a Varian 715-ES.

3. Results and discussion

3.1. Characterization of the cathode materials of spent Ni–MH batteries

Fig. 1 represents the micrographs of the cathode materials of spent Ni–MH batteries. Cracks are observed because of the variation in the molar volume and because of the increased internal pressure during repeated charge-and-discharge cycling. The predominant crystal structure of the Ni–MH cathode material is hexagonal. Fig. 2 shows the energy-dispersive X-ray (EDS) spectrum obtained from the positive electrode material. The presence of potassium from the KOH electrolyte is detected on the surface of the material. The presence of oxygen is due to Ni and Co oxides. The carbon and cobalt detected are used as additives to improve the electrical conductivity in the positive electrode. Fig. 3 shows the XRD results for the Ni–MH cathode material. The diffractogram shows peaks that, when compared with those reported in the JCPDS database, correspond to β-$Ni(OH)_2$ and $Co(OH)_2$, with lattice parameters of a = 3.13 Å and c = 4.61 Å. The structure of the compound CoOOH is also hexagonal; however, the lattice parameters are a = 2.86 Å and c = 8.81 Å. NiOOH exhibits an orthorhombic structure with parameters of a = 4.79 Å, b = 4.22 Å and c = 2.90 Å. The structure of NiO has a cubic structure [16–22]. ZnO and Mn_3O_4 are additives that stabilize the α-$Ni(OH)_2$ phase and improve the capacity of the electrodes, respectively. α-$Ni(OH)_2$ became β-$Ni(OH)_2$ during the charge-and-discharge cycling [23,24]. The composition and concentration of metal ions was determined by the dissolution of the cathode electrodes of Ni–MH batteries in

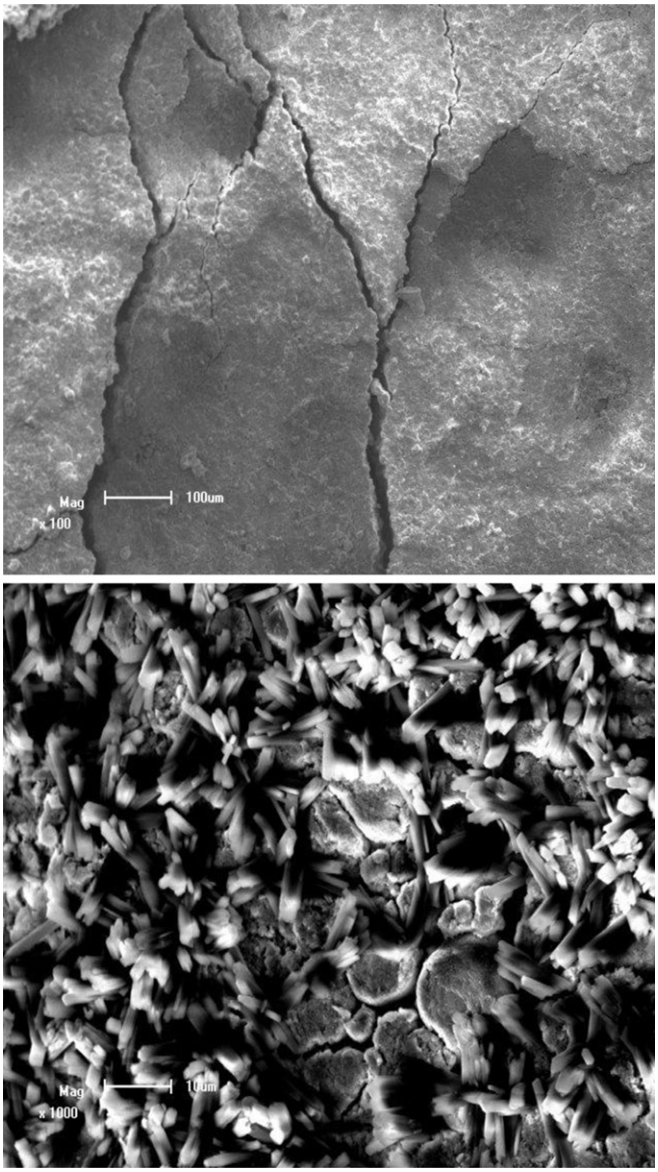

Fig. 1. Micrographs of the positive electrode of spent Ni–MH batteries.

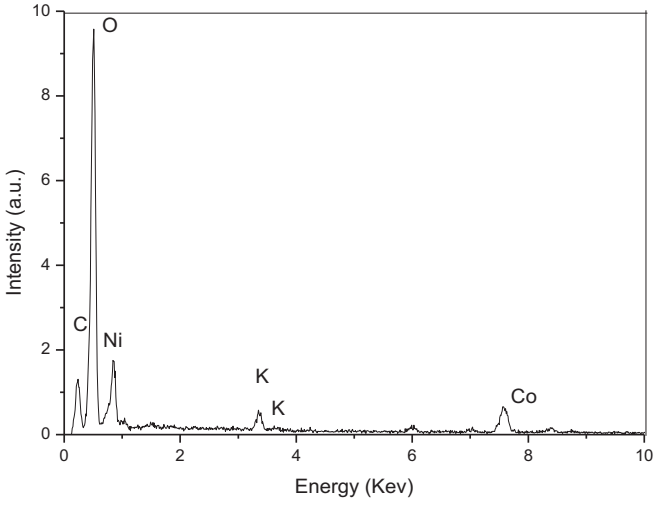

Fig. 2. Energy dispersive X-ray (EDX) spectrum obtained for the positive electrode of spent Ni–MH batteries.

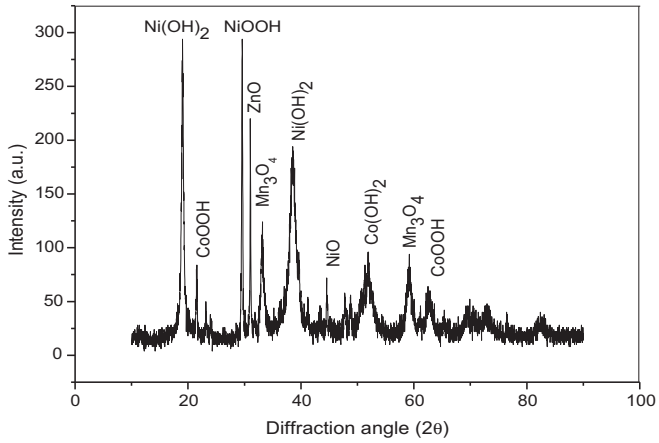

Fig. 3. Typical X-ray diffraction spectrum of a positive electrode from a spent Ni–MH battery.

aqua regia and by an analysis of the solution using the ICP-OES technique. The values of the concentrations of these ions in the solution are shown in Table 1. The concentration of nickel is relatively high, those of zinc and cobalt are moderate, and that of manganese is low. The presence of cerium and lanthanum is due to contamination from the negative electrode.

3.2. Characterization of materials recovered by chemical precipitation from cathodes of Ni–MH batteries

Fig. 4 shows the micrographs of the materials recovered from the cathodes. The micrographs of the recycled material show micropores lower than 2 nm, mesopores lower than 50 nm, and macropores greater than 50 nm. Fig. 5 shows the X-ray diffraction (XRD) spectrum of the materials recovered from the cathode of the Ni–MH battery. The diffractogram shows peaks that, when compared with the files in the JCPDS database, indicate a cell structure for the hexagonal system that corresponds to β-$Ni(OH)_2$ [18] and $Co(OH)_2$ [16]. The structure of $Zn(OH)_2$ is orthorhombic, with lattice parameters of $a = 8.49$ Å, $b = c = 5.16$ to 4.92 Å [25]. The structure of Mn_3O_4 is tetratagonal, with lattice parameters of $a = 5.76$ Å and $c = 9.44$ Å. Fig. 6 shows the infrared spectroscopy spectrum of the recovered materials. The stretching vibration of OH groups in the structures of β-$Ni(OH)_2$ and $Co(OH)_2$ is observed at 3646.9 cm^{-1}. The peaks in the wavenumber region from 1639.9 cm^{-1}–3443.3 cm^{-1} are attributed to angular deformation vibrations of water and to the stretching vibrations of the hydroxyl groups of absorbed and crystallized water. The Co–O, Ni–O and Mn–O vibrational stretches are observed in the wavenumber region between 461.38 cm^{-1} and 524.92 cm^{-1}. The band at 1384 cm^{-1} is attributed to the nitrate and carbonate ions in the precipitates.

The thermogravimetric curve shown in Fig. 7 indicates a mass loss of 17.57% ww^{-1} between the temperatures of 50 °C and 150 °C,

Table 1
ICP-OES analysis results for the solution of the positive electrode.

Element	Concentration mg L^{-1}	Concentration mmol L^{-1}
Ni	342.1	5.82
Zn	155.5	2.38
Co	146.5	2.49
Mn	26.4	0.401
Ce	0.61	0.00435
La	0.30	0.00216

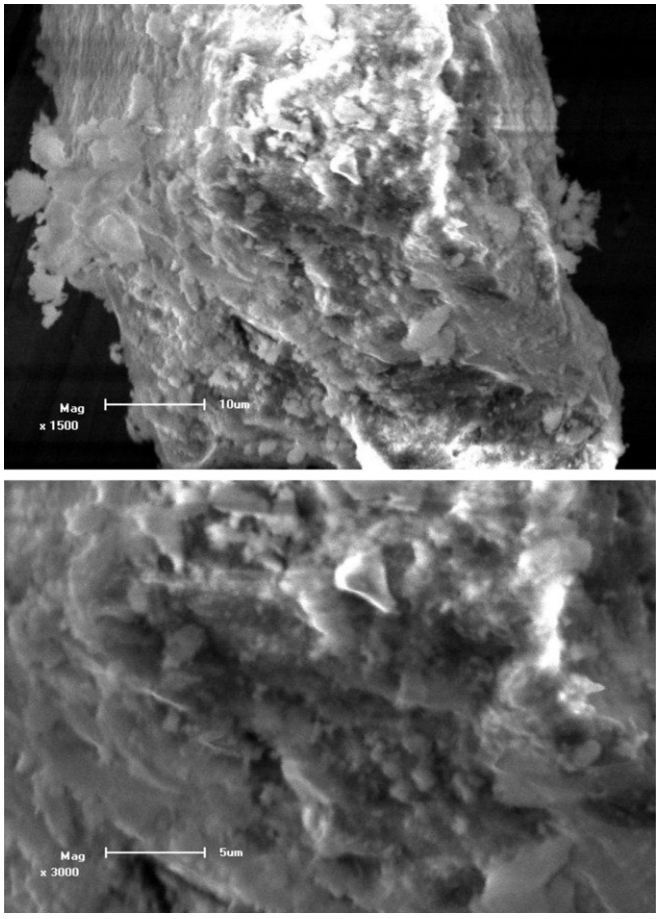

Fig. 4. Micrographs of the materials recovered by chemical precipitation.

which is attributed to the loss of adsorbed water. The 14.27% w w^{-1} mass loss between 150 °C and 365 °C is due to the removal of the nitrates and carbonates adsorbed onto the solid. The mass loss in the temperature range between 375 °C and 575 °C indicates that the anhydrous compounds undergo a dehydroxylation process. The oxides are thermodynamically stable at temperatures between 575 °C and 1200 °C.

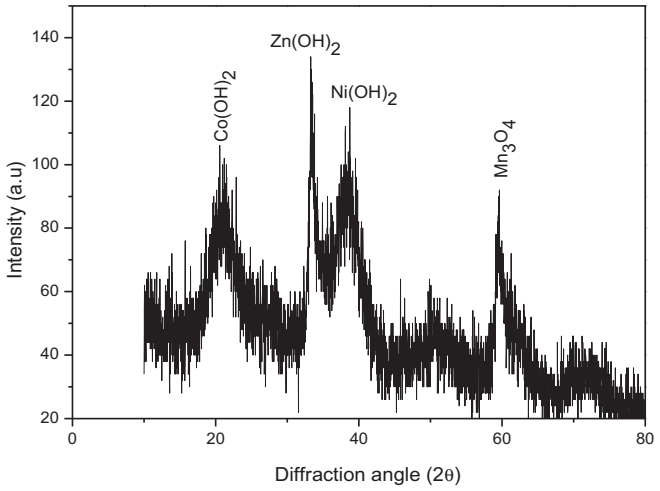

Fig. 5. X-ray diffraction spectrum of the materials recovered by chemical precipitation.

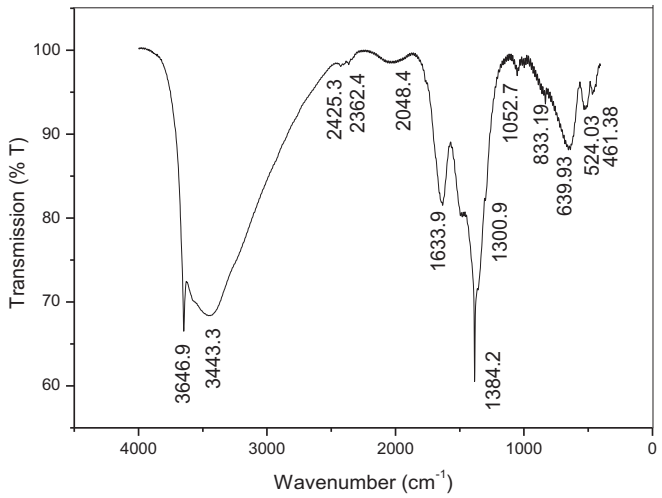

Fig. 6. Infrared spectroscopy spectrum of the materials recovered by chemical precipitation.

3.3. Electrochemical recycling of cathode materials from spent Ni–MH batteries

3.3.1. Cyclic voltammetric analysis of the formation of electrodeposits

Typical cyclic voltammetry traces performed at scan rates of 5.0 mV s^{-1}, 10.0 mV s^{-1}, and 20.0 mV s^{-1} are presented in Fig. 8. The voltammograms show a peak reduction between the potentials of −0.87 V and −0.96 V vs. Ag/AgCl. The peak current density in the reduction process is higher at scan rates of 5.0 mV s^{-1}. The intensity of the peak current density decreases in scans performed at rates faster than 10 mV s^{-1}, and a plateau is observed in which the current remains constant even when the potential becomes more cathodic. The decrease in the current density as the potential is varied can be explained by the formation and growth of hydroxide films. The hydroxide film formation occurs because of the metal/solution interface alkalinization, which is caused by the reduction reaction of the water. In the voltammograms, oxidation peaks appear at −0.09 V and −0.01 V vs. Ag/AgCl. The calculated area under the curve indicates that only a portion of the applied charge density was used to electrodeposit the electrodissolved materials.

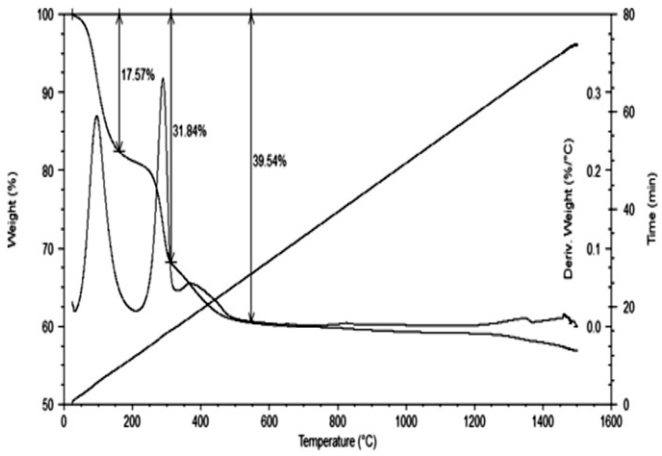

Fig. 7. Thermogravimetric curve for materials recovered by chemical precipitation; N_2 atmosphere (100 ml min^{-1}), scan rate of 10 °C min^{-1}, alumina crucible.

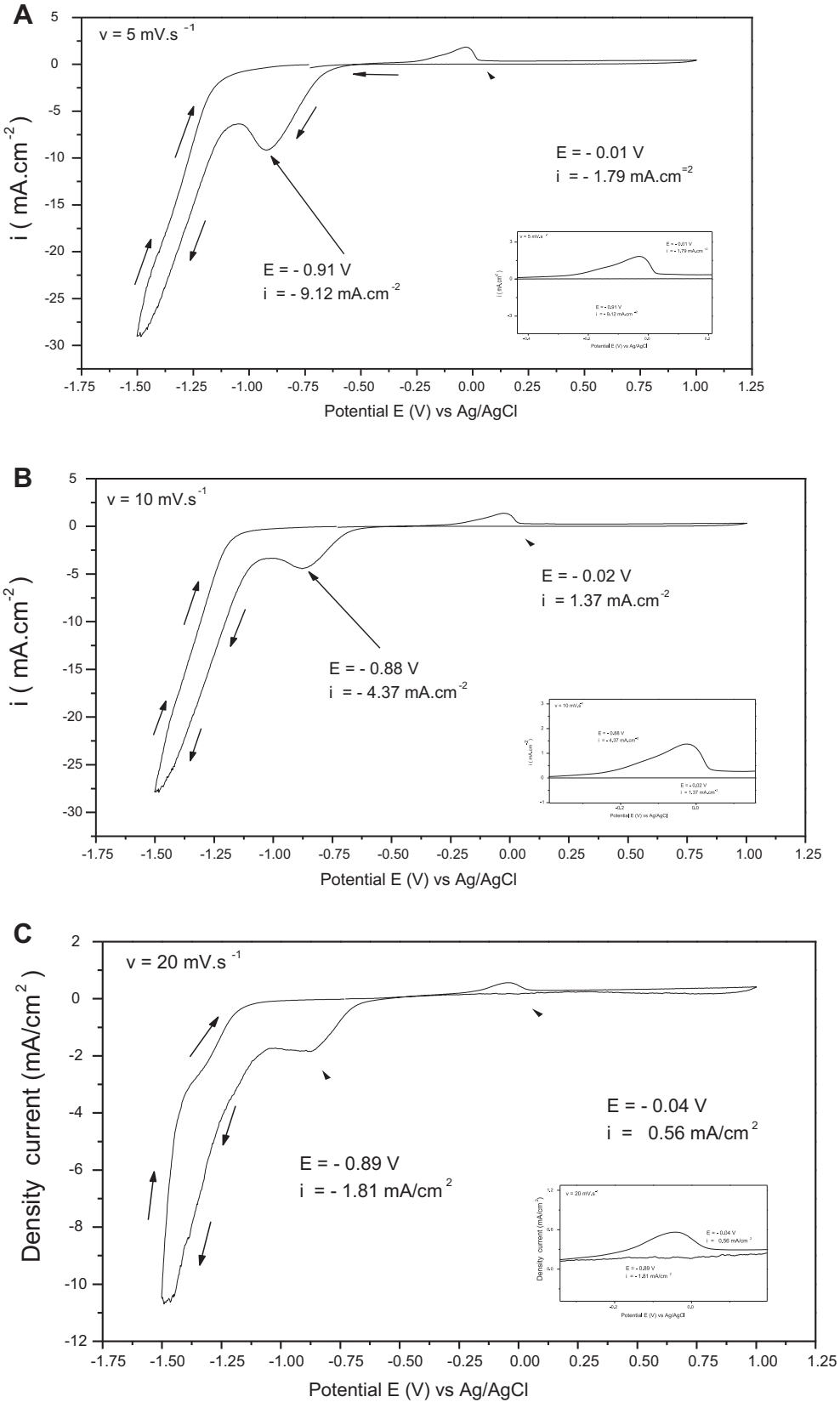

Fig. 8. Typical cyclic voltammograms performed at scans rates of 10.0 mV s^{-1}, 20.0 mV s^{-1}, 30.0 mV s^{-1}, 40.0 mV s^{-1} and 50.0 mV s^{-1}. Anodic peak in highlights.

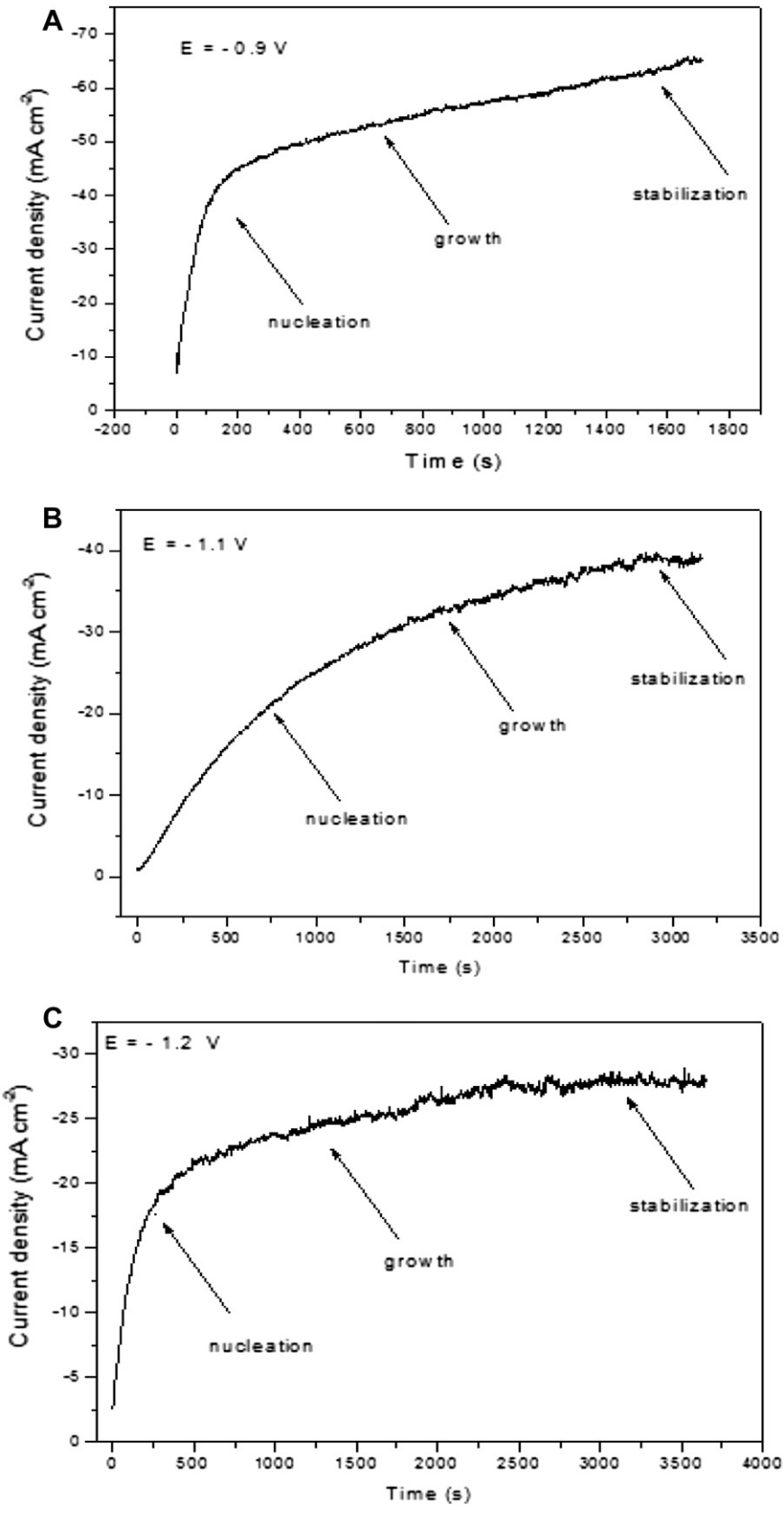

Fig. 9. Typical chronoamperograms for potentials of (A) −0.9 V, (B) −1.1 V, (C) −1.2 V vs. Ag/AgCl and at a charge density of −90.0 C cm^{-2}.

3.3.2. Potentiostatic analysis of the formation of the electrodeposits and their characterization

Typical chronoamperograms obtained for constant reduction potentials of −0.9 V, −1.1 V and −1.2 V vs. Ag/AgCl at a fixed charge density of −90.0 C cm^{-2} are shown in Fig. 9. The electrochemical potential values chosen for the chronoamperometric analysis are associated with the peak potentials, the patamar potential and the potential at which the current density increased due to the detachment of hydrogen, respectively. In general, the chronoamperograms exhibit three well-defined stages: (A) the initial stages of polarization, where a transient current density occurs due to the growth of the first nucleation sites at the metal–solution interface, (B) the second stage, where growth of the electrodeposits occurs, and (C) the third stage, where the current density stabilization is observed in the final moments when the electrodeposition process is controled by diffusion. The amounts of Ni^{2+}, Co^{2+}, Zn^{2+} and Mn^{2+} electrodeposited during the application of constant potentials of −0.9 V, −1.1 V and −1.2 V vs. Ag/AgCl at a fixed charge density −90.0 C cm^{-2} were obtained via the dissolution of the coating in aqua regia, and the solutions were analysed using the ICP-OES technique; the results are presented in Table 2. The proportion of electrodeposited nickel is greater than that of the other metals and is independent of the applied potential. The concentration of cobalt is, on average, fifteen times less than that of nickel. The concentration of manganese is lower than that of cobalt, and zinc was not detected. Although the system is not under equilibrium conditions, the theoretical potential was calculated using the Nernst equation based on the concentrations of metal ions from the dissolved cathode of the battery. The reduction potentials of Ni^{2+}, Co^{2+}, Zn^{2+} and Mn^{2+} with respect to an Ag/AgCl reference electrode are −0.54 V, −0.57 V, −1.06 V, and −1.60 V, respectively. In accordance with the calculations of the theoretical potentials, the electrodeposition of Ni^{2+}, and Co^{2+} should occur first because because their reduction potential are the least cathodic, and Zn^{2+} eletrodeposition should occur before Mn^{2+} electrodeposition. The amount of nickel ions deposited is related to the composition of the electroplating bath that contains 0.4 mol L^{-1} boric acid and 0.3 mol L^{-1} ammonium sulfamate. Sulfamate baths that contain boric acid have a high deposition rate of nickel and form thick deposits with low internal stress [26,27]. Another important factor is that the reaction of hydrogen detachment that occurs in parallel with the reduction of metal ions causes alkalinization at the metal–solution interface. Consequently, the

Table 2
ICP-OES analysis results for the solution of the electrodeposits.

Element	Mass $E = -0.9$ V (mg L^{-1})	Mass $E = -1.1$ V (mg L^{-1})	Mass $E = -1.2$ V (mg L^{-1})
Ni	6.922	10.57	5.173
Co	0.361	0.715	0.367
Mn	0.002	0.123	0.018
Zn	Not detected	Not detected	Not detected

Table 3
The charge efficiency for the electrodeposits.

Element	Charge density $E = -0.9$ V (C cm^{-2})	Charge density $E = -1.1$ V (C cm^{-2})	Charge density $E = -1.2$ V (C cm^{-2})
Ni	45.6	69.8	34.0
Co	3.64	4.68	2.40
Mn	0.0141	0.86	0.127
Zn	Not detected	Not detected	Not detected
Charge efficience (%)	54.7	83.7	40.6

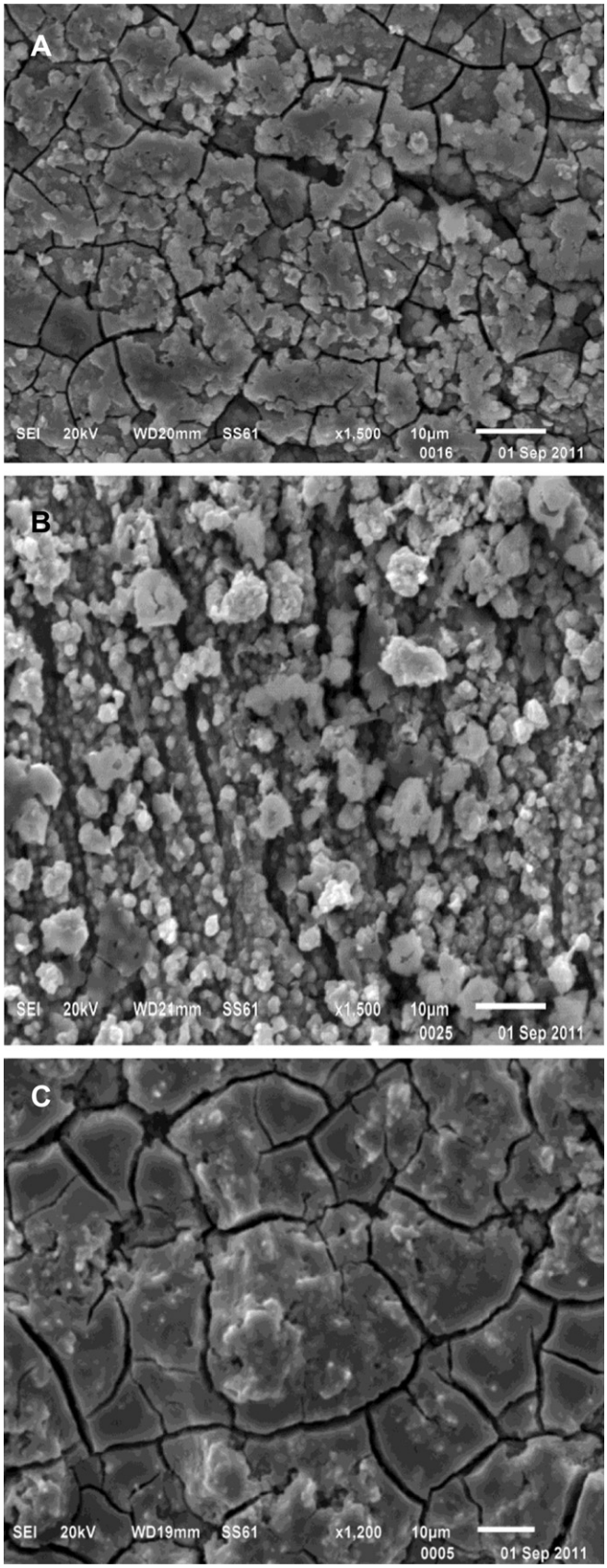

Fig. 10. Micrographs of the surface of the coatings obtained at constant potentials of −0.9 V, −1.1 V and −1.2 V vs. Ag/AgCl and at a charge density −90.0 C cm^{-2}.

possibility arises of the formation of hydroxides of nickel, cobalt, zinc and manganese on the electrodes. The nickel ions form a stable complex with the sulfamate anions. The formation of the complex prevents the precipitation of nickel hydroxide. Zinc can, depending on the pH at the metal–solution interface, form soluble complexes, such as $[Zn(OH)_4]^{2-}$. $[Zn(OH)_4]^{2-}$ is not reduced in the potential range investigated in this work [28]. Therefore, the presence of zinc in the electrodeposits was not detected. The presence of

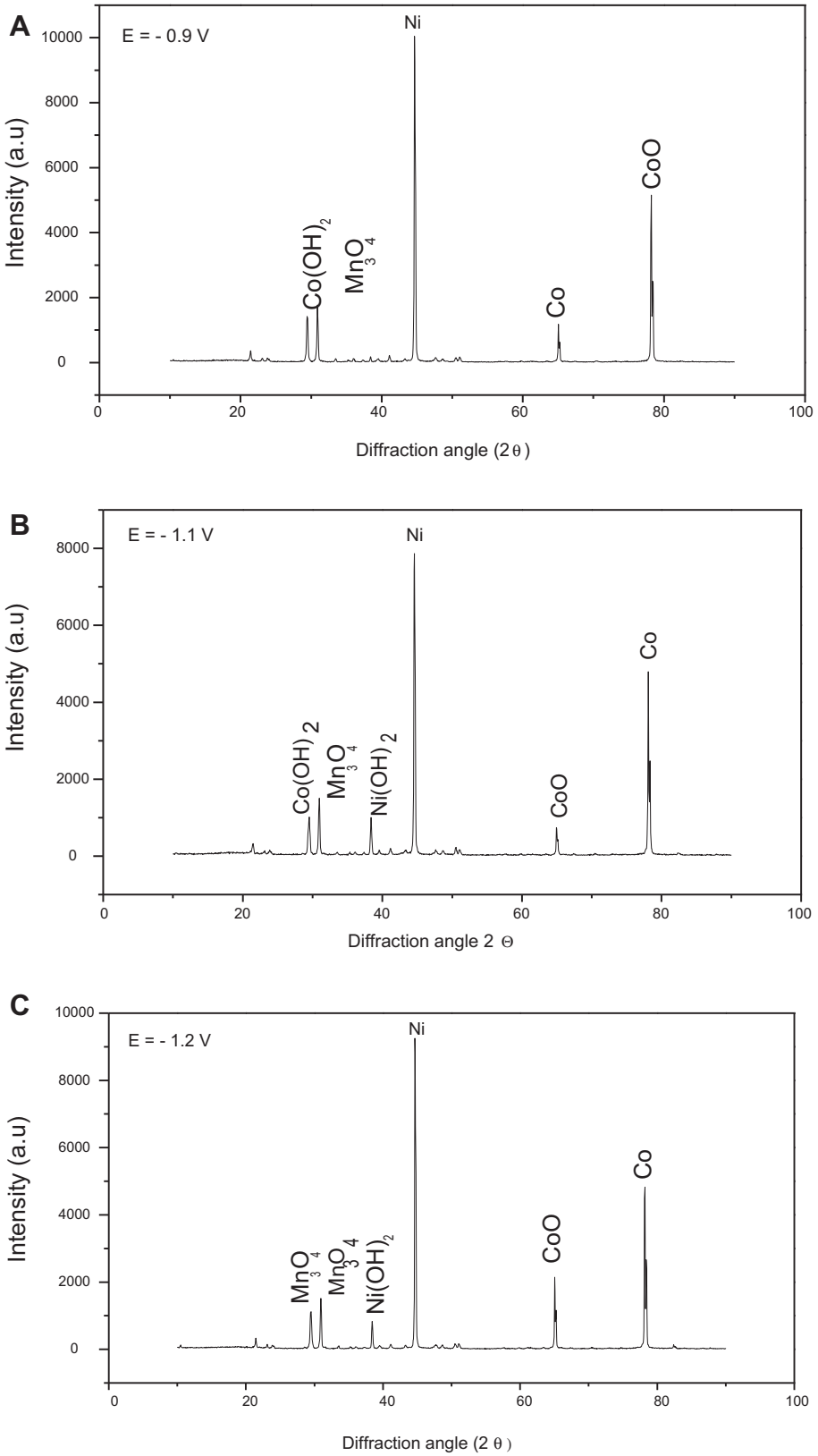

Fig. 11. X-ray diffractograms of the electrodeposits obtained at potentials of (A) −0.9 V, (B) −1.1 V, and (C) 1.2 V vs. Ag/AgCl.

manganese in the electrodeposits results from the precipitation of manganese hydroxide. The results summarized in Table 3 indicate that a charge efficiency of 83.7% is obtained for the electrodeposits formed by the application of a constant potential of −1.1 V vs. Ag/AgCl at a fixed charge density of −90 C cm^{-2}. To complete the characterization, we collected micrographs of the electrodeposits. Fig. 10 shows a micrograph of the surface of the coatings obtained at constant potentials of −0.9 V, −1.1 V and −1.2 V vs. Ag/AgCl at a fixed charge density of −90.0 C cm^{-2}. The electrodeposits formed at an applied potential of −1.1 V are more homogeneous and have fewer cracks than those formed at −0.9 V and −1.2 V. Fig. 11 shows the X-ray diffractograms of the electrodeposits obtained at potentials of −0.9 V, −1.1 V and −1.2 V vs. Ag/AgCl. The peaks in the X-ray diffractogram, when compared with those listed in the JCPDS database, allow the identification of the structures of Ni [29], Co [30], $Co(OH)_2$ [16], and Mn_3O_4 [19]. The peaks are observed at similar 2θ diffraction angles, which indicates that the electrodeposits have the same crystal structures. A comparison of Fig. 11A with Fig. 11B and C reveals that more-cathodic potentials of −1.1 V and −1.2 V vs. Ag/AgCl result in the precipitation of nickel hydroxide.

3.4. Cyclic voltammetric analysis of the electrodissolution of the electrodeposits obtained under potentiostatic conditions

Linear voltammetry was used to investigate the oxidation process of the electrodeposits obtained under a constant potential. The voltammetry was performed in a solution of 0.5 mol L^{-1} Na_2SO_4 to prevent the chemical dissolution of the coatings. The potential scans were initiated from the open-circuit potential to the anodic region of 1.5 V at a scan rate of 5.0 mV s^{-1} Fig. 12A shows only one anodic peak (denominated as peak I) at 0.24 V due to the dissolution of nickel and cobalt. The calculated area under the curve of the graph indicates a charge density of 4.86 C cm^{-2}, which shows that only a portion of the applied charge density was used for electrodissolution of the electrodeposited material. Fig. 12B represents the voltammogram for the electrodissolution of the electrodeposit formed at a constant potential of −1.1 V. Two anodic peaks are observed at −0.37 V (peak II) and at 0.33 V (peak I). Peak I, at potential of 0.33 V, is attributed to the electrodissolution of nickel and cobalt. The authors of previous works have confirmed, using an electrochemical crystal quartz microbalance, that the reduction of cobalt under acidic pH conditions occurs with the formation of adsorbed hydrogen ions (CoH^+) [31]. Peak II, at −0.37 V, is due to the desorption of the hydrogen adsorbed onto the cobalt. The calculation of the absolute area under the curve of the graph results in a charge density of 19.22 C cm^{-2} Fig. 12C represents the voltammogram for electrodissolution of the electrodeposit formed at a constant potential of −1.2 V. A shoulder is observed between 0.4 V and 0.0 V because of the desorption of hydrogen adsorbed onto cobalt, and a peak I at 0.25 V is observed due to the dissolution of nickel and cobalt. Potentials more positive than 0.64 V induce an increase in the current density to between 31.54 mA cm^{-2} and 130 mA cm^{-2}. The charge density of 48.23 C cm^{-2} corresponds to the oxidation of cobalt and nickel compounds and to water oxidation, thus leading to oxygen detachment. Two facts should be highlighted in the voltammetry results. The density of the anodic charge increases as the deposition potential becomes more cathodic. The intensity of peak I increases with the definition of the anodic peak II. Therefore, the process that occurs in anodic peak I is related to the existence of peak II. Based on these electrochemical results, we propose the following mechanism: i. Anodic peak I indicates the dissolution of nickel and cobalt:

$$Ni \rightarrow Ni^{2+} + 2e \quad (1)$$

$$Co \rightarrow Co^{2+} + 2e \quad (2)$$

ii. In anodic peak II (figure B), the hydrogen ions desorb, which causes an increase in acidity at the metal–solution interface, as described in equation (3):

$$CoH^{+}_{ads} \rightarrow Co + H^{+} \quad (3)$$

The increase in the acidity at the metal–solution interface facilitates the dissolution of nickel and cobalt, which, in this case,

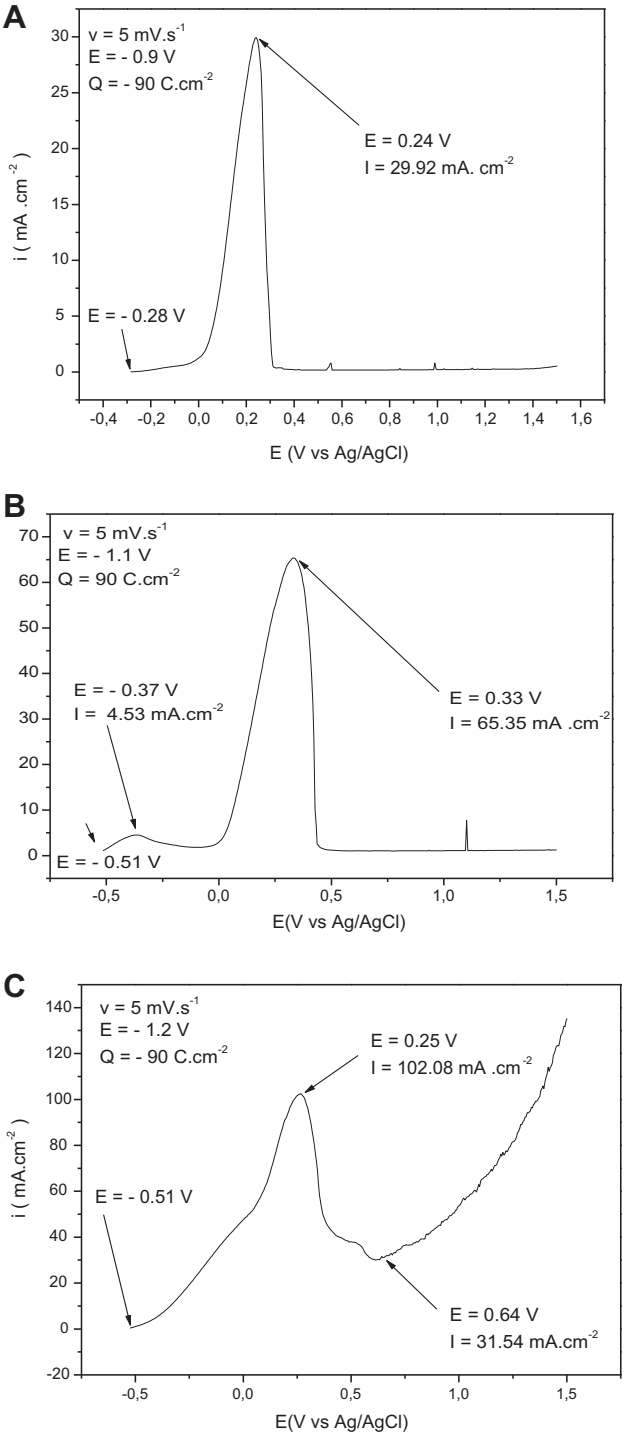

Fig. 12. Linear voltammograms of the dissolution of the electrodeposits performed at constant potentials of (A) −0.9 V, (B) −1.1 V, and (C) −1.2 V vs. Ag/AgCl.

results in an increase in the charge density of peak I. The reactions described by equations (1)–(3) can occur simultaneously, as shown in Fig. 12C, where the first peak is not set, and a sharp increase is observed in the current density after the second peak due to the oxidation of water.

4. Conclusions

The materials recovered by chemical precipitation are composed of β-$Ni(OH)_2$, $Co(OH)_2$, $Zn(OH)_2$ and Mn_3O_4. Zinc and manganese are additives that improve the capacity of the electrodes. The infrared spectroscopy spectrum of the recovered materials revealed a band at 1384 cm^{-1}, which is attributed to nitrate and carbonate ions from mother solutions adsorbed onto the precipitates. The TGA trace shows that the mass loss of 17.57% ww^{-1} between the temperatures of 50 °C and 150 °C is due to the loss of adsorbed water. The 14.27% ww^{-1} mass loss at temperatures between 150 °C and 365 °C is due to the removal of nitrates and carbonates adsorbed onto the solid. In the temperature range from 375 °C to 575 °C, the mass–loss curves show that the anhydrous compounds undergo a dehydroxylation process. The oxides are thermodynamically stable at temperatures between 575 °C and 1200 °C.

The electrochemical recycling of cathode materials from spent Ni–MH batteries were studied using cyclic voltammetry at scan rates of 10.0 mV s^{-1}, 20.0 mV s^{-1}, 30.0 mV s^{-1}, 40.0 mV s^{-1} and 50.0 mV s^{-1}. The current density peaks in the reduction process were observed to be more intense at scan rates of 1.0 mV s^{-1} and 5.0 mV s^{-1}. The intensity of the current density decreases at scan rates of 10 mV s^{-1} and higher. The decrease in the current density with the increasing potential is explained by the formation and growth of hydroxide films. The formation of the hydroxide films is due to the alkalinization of the metal–solution, which is caused by the reduction reaction of water. The amounts of Ni^{2+}, Co^{2+}, Zn^{2+} and Mn^{2+} that was electrodeposited under applied constant potentials of −0.9 V, −1.1 V and −1.2 V vs. Ag/AgCl and at a fixed charge density of −90.0 C cm^{-2} were obtained using the ICP-OES technique. The amount of deposited nickel ions is related to the composition of the electroplating bath that contains 0.4 mol L^{-1} boric acid and 0.3 mol L^{-1} ammonium sulfamate. The nickel ions form a stable complex with the sulfamate anions, which prevents the precipitation of nickel hydroxide. The presence of zinc was not detected in the electrodeposits because the ion $[Zn(OH)_4]^{2-}$ does not undergo reduction in the potential range investigated in this work. The presence of manganese in the electrodeposits is due to the precipitation of manganese hydroxide. The X-ray diffractograms allowed the identification of the structures of Ni, CoO, $Co(OH)_2$, and Mn_3O_4. Linear voltammetry was used to investigate the dissolution of the electrodeposits obtained at constant potentials. The dissolution of the electrodeposits depended on the applied potential. Only one anodic peak potential, at 0.24 V, was observed due to the dissolution of nickel and cobalt during the electrodeposition performed at a constant potential of −0.9 V. Two anodic peaks, at −0.37 V and 0.33 V, were observed for the electrodeposition formed at a constant potential of −1.1 V. The peak at −0.37 V was attributed to the desorption of hydrogen adsorbed onto cobalt. The peak at 0.33 V was due to the electrodissolution of nickel and cobalt. A shoulder was observed between 0.4 V and 0.0 V for the electrodissolution of the electrodeposit formed at constant potential of −1.2 V due to desorption of hydrogen adsorbed on cobalt, which partially overlapped a peak observed at 0.25 V attributed to the dissolution of nickel and cobalt. Potentials more positive than 0.64 V resulted in an increase in the current density, which corresponds to the oxidation of cobalt and nickel compounds and to the oxidation of water, thus causing oxygen detachment.

Acknowledgements

The authors acknowledge MCT–CNPq–FAPES and CAPES for financial support.

References

[1] K. Scott, Nickel–Metal Hydride Batteries, Encyclopedia of Electrochemical Power Sources, Elsevier, New York, 2009, pp. 198–208.
[2] I. Vassura, L. Morselli, E. Bernardi, F. Passarini, Waste Manage. 29 (2009) 2332–2335.
[3] T.K. Yinga, X.P. Gaob, W.K. Huc, F. Wud, D. Noréusc, Int. J. Hydrogen Energy 31 (2006) 525–530.
[4] L. Pietrelli, B. Bellomo, D. Fontana, M. Montereali, Waste Manage. 25 (2005) 221–226.
[5] Status of life cycle inventories for batteries J.L. Sullivan, L. Gaines, Energy Convers. Manage. 58 (2012) 134–148.
[6] J. Nan, D. Han, M. Yang, M. Cui, X. Hou, Hydrometallurgy 84 (2006) 75–80.
[7] P. Zhang, T. Yokoyama, O. Itabashi, Y. Wakui, T.M. Suzuki, K. Inoque, J. Power Sources 77 (1999) 116–122.
[8] T. Muller, B. Friedrich, J. Power Sources 158 (2006) 1498–1509.
[9] C. Lupi, D. Pilone, Waste Manage. 22 (2002) 871–874.
[10] L. Li, S. Xu, Z. Ju, F. Wu, Hydrometallurgy 100 (2009) 41–46.
[11] J.A.S. Tenorio, D.C.R. Espinosa, J. Power Sources 108 (2002) 70–73.
[12] M.A. Rabah, F.E. Farghaly, M.A. Abd-El Motaleb, Waste Manage. 28 (2008) 1159–1167.
[13] P. Zhang, T. Yokoyama, O. Itabashi, Y. Wakui, T.M. Suzuki, K. Inoue, Hydrometallurgy 50 (1998) 61–75.
[14] L.E.O.C. Rodrigues, M.B. Mansur, J. Power Sources 195 (2010) 3735–3741.
[15] D.C.R. Espinosa, A.M. Bernardes, J.A.S. Tenório, J. Power Sources 135 (2004) 311–319.
[16] Joint Committee on Powder Diffraction Standards, Diffraction Data File, No. 2–1094, JCPDS International Center for Diffraction Data, Pennsylvania, 1991.
[17] Joint Committee on Powder Diffraction Standards, Diffraction Data File, No. 14–117, JCPDS International Center for Diffraction Data, Pennsylvania, 1991.
[18] Joint Committee on Powder Diffraction Standards, Diffraction Data File, No. 16–154, JCPDS International Center for Diffraction Data, Pennsylvania, 1991.
[19] Joint Committee on Powder Diffraction Standards, Diffraction Data File, No. 26–1107, JCPDS International Center for Diffraction Data, Pennsylvania, 1991.
[20] Joint Committee on Powder Diffraction Standards, Diffraction Data File, No. 27–956, JCPDS International Center for Diffraction Data, Pennsylvania, 1991.
[21] Joint Committee on Powder Diffraction Standards, Diffraction Data File, No. 3–752, JCPDS International Center for Diffraction Data, Pennsylvania, 1991.
[22] Joint Committee on Powder Diffraction Standards, Diffraction Data File, No. 47–1049, JCPDS International Center for Diffraction Data, Pennsylvania, 1991.
[23] P. Oliva, J. Leonardi, J.F. Laurent, C. Delmas, J.J. Braconnier, M. Figlaz, F. Fievet, A. de Guibert, J. Power Sources 8 (1982) 229–255.
[24] M.B.J.G. Freitas, R.K. Silva e Silva, D.M. Anjos, A. Rozario, P.G. Manoel, J. Power Sources 163 (2007) 1114–1119.
[25] Joint Committee on Powder Diffraction Standards, Diffraction Data File, No. 38–385, JCPDS International Center for Diffraction Data, Pennsylvania, 1991.
[26] D. Golodnitsky, Yu. Rosenberg, A. Ulus, Electrochim. Acta 47 (2002) 2707–2714.
[27] M. Saitou, S. Oshiro, S.M. Asadul Hossain, J. Appl. Electrochem. 38 (2008) 309–313.
[28] M.B.J.G. Freitas, M.K. de Pietre, J. Power Sources 143 (2005) 270–274.
[29] Joint Committee on Powder Diffraction Standards, Diffraction Data File, No. 01–1258, JCPDS International Center for Diffraction Data, Pennsylvania, 1991.
[30] Joint Committee on Powder Diffraction Standards, Diffraction Data File, No. 05–0727, JCPDS International Center for Diffraction Data, Pennsylvania, 1991.
[31] M.B.J.G. Freitas, E.M. Garcia, J.S. Santos, E.C. Pereira, J. Power Sources 185 (2008) 549–553.